Article

Cell

# Single-Molecule Imaging Reveals that Argonaute Reshapes the Binding Properties of Its Nucleic Acid Guides

## Graphical Abstract

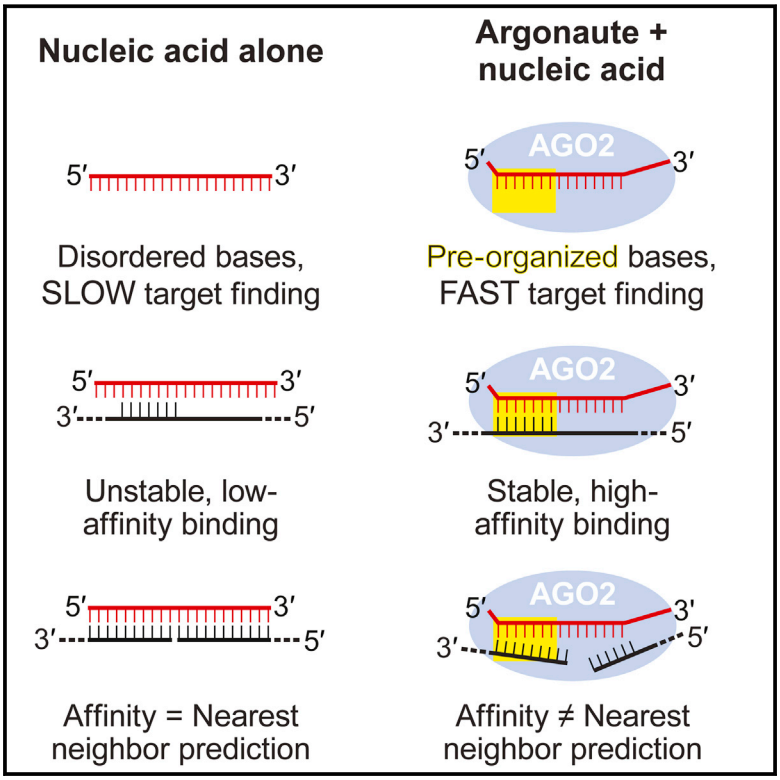


## Highlights

- Argonaute changes the rate of target finding by pre-organizing a region of its guide
- Seed pairing is required for rapid target finding and stable binding
- AGO2 releases its cleaved products by destabilizing their interaction with the guide
- RISC makes its guide behave more like an RNA-binding protein and less like free RNA

## Authors

William E. Salomon, Samson M. Jolly, Melissa J. Moore, Phillip D. Zamore, Victor Serebrov

## Correspondence

phillip.zamore@umassmed.edu (P.D.Z.), victor.serebrov@umassmed.edu (V.S.)

## In Brief

Argonaute proteins reshape how oligonucleotides find, bind, and dissociate from complementary nucleic acid sequences. By re-writing the rules, Argonautes allow oligonucleotides to serve as specificity determinants with thermodynamic and kinetic properties more typical of RNA-binding proteins.

Salomon et al., 2015, Cell *162*, 84–95
July 2, 2015 
http://dx.doi.org/10.1016/j.cell.2015.06.029

CellPress

Cell

Article

# Single-Molecule Imaging Reveals that Argonaute Reshapes the Binding Properties of Its Nucleic Acid Guides

William E. Salomon,[1] Samson M. Jolly,[1] Melissa J. Moore,[1] Phillip D. Zamore,[1,*] and Victor Serebrov[1,*]
[1]RNA Therapeutics Institute, Howard Hughes Medical Institute, and Department of Biochemistry & Molecular Pharmacology, University of Massachusetts Medical School, Worcester, MA 01605, USA
*Correspondence: phillip.zamore@umassmed.edu (P.D.Z.), victor.serebrov@umassmed.edu (V.S.)
http://dx.doi.org/10.1016/j.cell.2015.06.029

## SUMMARY

**Argonaute proteins repress gene expression and defend against foreign nucleic acids using short RNAs or DNAs to specify the correct target RNA or DNA sequence. We have developed single-molecule methods to analyze target binding and cleavage mediated by the Argonaute:guide complex, RISC. We find that both eukaryotic and prokaryotic Argonaute proteins reshape the fundamental properties of RNA:RNA, RNA:DNA, and DNA:DNA hybridization—a small RNA or DNA bound to Argonaute as a guide no longer follows the well-established rules by which oligonucleotides find, bind, and dissociate from complementary nucleic acid sequences. Argonautes distinguish substrates from targets with similar complementarity. Mouse AGO2, for example, binds tighter to miRNA targets than its RNAi cleavage product, even though the cleaved product contains more base pairs. By re-writing the rules for nucleic acid hybridization, Argonautes allow oligonucleotides to serve as specificity determinants with thermodynamic and kinetic properties more typical of RNA-binding proteins than of RNA or DNA.**

## INTRODUCTION

MicroRNAs (miRNAs) and small interfering RNAs (siRNAs) direct Argonaute proteins to repress cellular mRNAs and silence viruses and transposons. In animals, siRNAs typically direct target cleavage, whereas miRNAs guide target binding, allowing Argonaute to recruit proteins that trigger exonucleolytic RNA degradation or inhibit translational initiation or elongation (Huntzinger and Izaurralde, 2011). Argonaute proteins comprise three distinct domains (Song et al., 2004). The Mid domain binds the 5′ phosphate of the guide RNA, anchoring it to the protein (Wang et al., 2008b). The PAZ domain binds the 3′ end of the guide, facilitating Argonaute loading (Song et al., 2003; Lingel et al., 2004; Ma et al., 2004; Tomari and Zamore, 2005). The PIWI domain catalyzes target cleavage (Liu et al., 2004; Martinez and Tuschl, 2004; Schwarz et al., 2004; Wang et al., 2008a; Wang et al., 2009b; Schirle et al., 2014). Some animal Argonaute proteins contain an additional N-terminal domain that prevents base pairing of the target to the guide beyond guide position g16 (Kwak and Tomari, 2012; Faehnle et al., 2013; Hauptmann et al., 2013).

Animal miRNAs bind their targets via guide nucleotides g2–g8 (Lewis et al., 2003; Rajewsky and Socci, 2004; Krek et al., 2005; Lewis et al., 2005; Lim et al., 2005). Argonaute pre-organizes these "seed" nucleotides into a conformation favorable for base pairing (Ma et al., 2004; Parker et al., 2005; Wang et al., 2008b; Elkayam et al., 2012; Nakanishi et al., 2012), pre-paying the entropic penalty inherent in base pairing to a target (Parker et al., 2009). Consequently, the seed sequence determines the binding specificity of Argonaute.

siRNAs generally base pair more extensively to their target RNAs than miRNAs. In mammals, only AGO2 can cleave RNA (Faehnle et al., 2013; Hauptmann et al., 2013). Efficient endonucleolytic cleavage of a target—always between target nucleotides t10 and t11—requires that the guide base pairs at least five to eight nucleotides beyond the seed; "zippering" of the guide:target helix allows the enzyme to attain a catalytically competent conformation but provides little additional binding energy (Elbashir et al., 2001a; Elbashir et al., 2001b; Haley and Zamore, 2004; Rivas et al., 2005; Ameres et al., 2007; Wang et al., 2008a; Wang et al., 2009a).

The fundamental properties of ~21 nt RNA oligomers make them poor guides for directing gene regulation. Single-stranded, 5′ monophosphorylated RNA is readily degraded by endo- and exonucleases and can form intra- and intermolecular structures that inhibit target binding. At physiological temperature, pH, and ionic strength, 21 nt RNA oligomers bind with little specificity, accommodating insertions, deletions, and mismatches, and sub-sequences > 12 nt can hybridize stably to complementary sites (Herschlag, 1991). Moreover, the rate of RNA and DNA hybridization is limited by the rate of successful collisions that convert to stable binding events (Ross and Sturtevant, 1960; Ross and Sturtevant, 1962; Nygaard and Hall, 1964; Wetmur and Davidson, 1968). This slow on-rate ($k_{on}$) means that the search for complementary targets is rate determining. Once formed, 21 bp RNA:RNA duplexes are nearly irreversible in physiological conditions: a fully base-paired double-stranded RNA composed of let-7a and its complement is predicted to have a $K_D = 2.3 \times 10^{-16}$ nM, implying a $k_{off} = 2.1 \times 10^{-18}$ $s^{-1}$ ($\tau = \sim 1.5 \times 10^{10}$ years). In contrast, an 8 bp duplex formed with just the let-7a seed sequence is less stable—the predicted

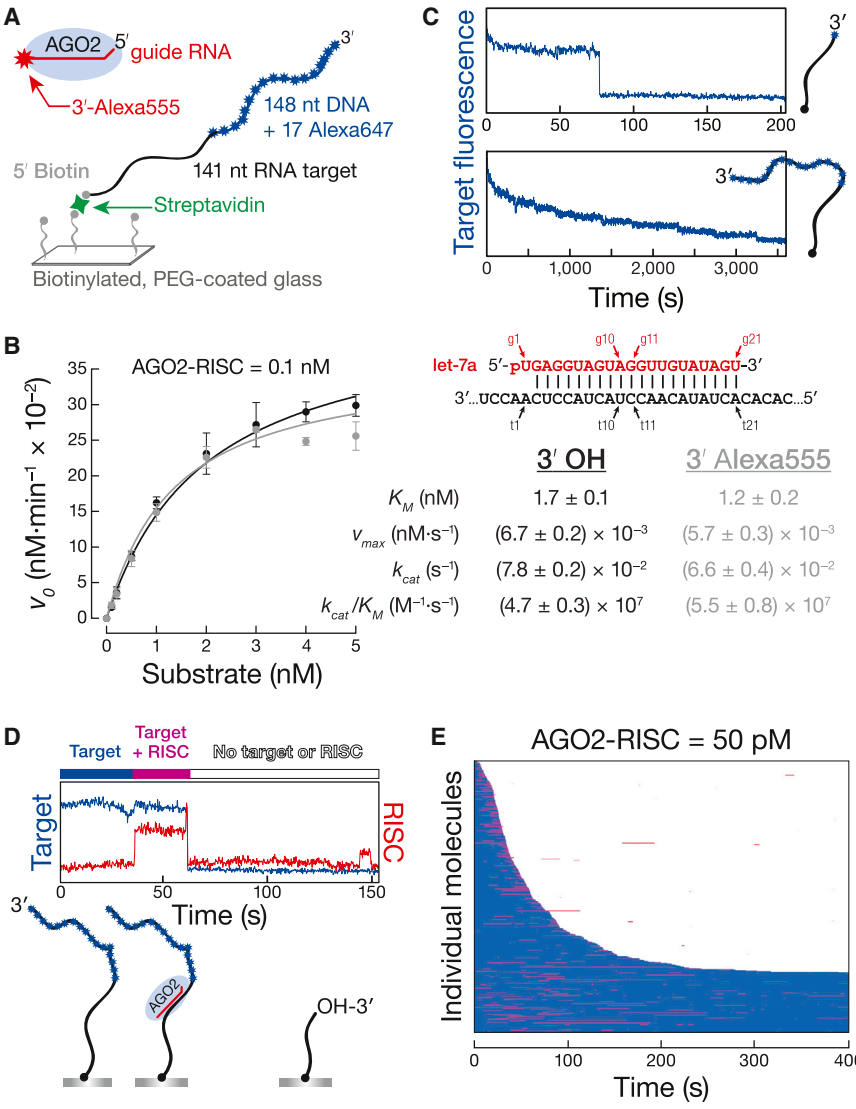


**Figure 1. Single-Molecule Analysis of Nucleic Acid-Guided Argonaute Proteins**

(A) Strategy to measure RNA- or DNA-guided Argonaute interactions with RNA or DNA targets.

(B) Standard ensemble Michaelis-Menten analysis of target cleavage for an RNA guide and a 3′ Alexa555-labeled RNA guide. Mean ± SD (n = 3).

(C) Unlike target with a single Alexa647 dye, the stepwise photobleaching of a target with 17 Alexa647 dyes is readily distinguished from target cleavage.

(D) A trace of an individual molecule of target RNA undergoing RNAi catalyzed by mouse AGO2 with a let-7a RNA guide. Colored bars above trace summarize the species observed here and in the rastergrams.

(E) Color-coded rastergram representation of let-7a-guided AGO2 binding and cleaving a fully complementary RNA target. The rastergram presents 426 individual RNA target molecules, each in a single row.

See also Figure S1 and Movies S1, S2, S3, and S4.

$K_D$ = 21 μM implies a $k_{off}$ = 0.094 s$^{-1}$ (τ = ~11 s). Argonaute proteins change all of these properties of nucleic acids.

We sought to understand how Argonaute proteins overcome the limitations inherent in their guides. Here, we show that Argonaute proteins reshape the fundamental properties of RNA:RNA, RNA:DNA, and DNA:DNA hybridization. Once bound to Argonaute, a small RNA or DNA guide no longer follows the well-established rules for finding, binding, and dissociating from complementary nucleic acid sequences. By re-writing the rules, Argonautes convert oligonucleotides into specificity determinants with thermodynamic and kinetic properties more typical of RNA-binding proteins than of nucleic acids.

## RESULTS

To measure the properties of RISC, we used multi-color, total internal reflection fluorescence microscopy to excite only those fluorescent molecules immediately above the slide surface (Friedman et al., 2006). Alexa647-labeled target RNA was attached to a glass surface and then incubated with purified RISC containing a 3′ Alexa555-labeled guide strand (Figure 1A). Dye addition did not meaningfully affect the activity of mouse AGO2 guided by let-7a RNA—standard ensemble experiments found similar $K_M$ (1.7 ± 0.1 nM versus 1.2 ± 0.2 nM) and $k_{cat}$ (7.8 ± 0.2 × 10$^{-2}$ sec$^{-1}$ versus 6.6 ± 0.4 × 10$^{-2}$ sec$^{-1}$) values for unmodified and 3′ Alexa555-labeled guides (Figures 1B and S1A). Furthermore, $K_M$ values agree well with that of human AGO2-RISC (mouse AGO2 is 99% similar to human AGO2, differing only in seven N-terminal amino acids; Martinez and Tuschl, 2004; Rivas et al., 2005; Ameres et al., 2007).

To distinguish photobleaching from target cleavage, we constructed a 141 nt RNA target containing 17 Alexa647 dyes within a 148-nt DNA 3′ extension. The brightness of this target allowed us to reduce laser power, which decreased the photobleaching rate and permitted long observation times (Figure 1C and Supplemental Experimental Procedures). The resulting stepwise photobleaching of multiple Alexa647 dyes was readily distinguishable from the all-or-none fluorescence change caused by target cleavage and 3′ product release.

### RISC Changes the Rate-Determining Step for Nucleic Acid Hybridization

Pre-organization by Argonaute of the seed sequence into a stacked conformation has been proposed to make productive collisions with target more likely. The association rate constant, $k_{on}$, for mammalian AGO2 has been inferred from $K_D$ and $k_{off}$

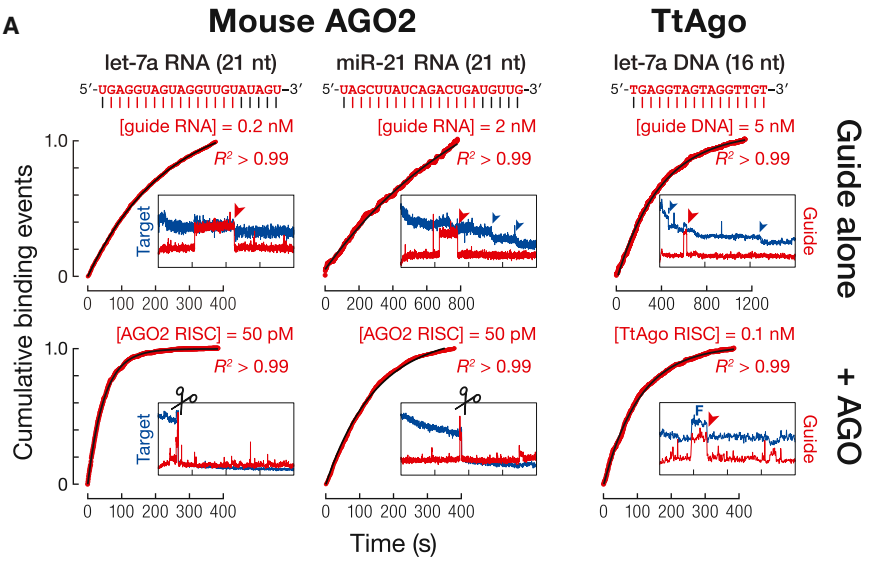


**Figure 2. Argonaute Accelerates Guide Binding to Target**

(A) Comparison of target binding rates ($k_{on}$) by 21 nt RNA-guided mouse AGO2- and 16 nt DNA-guided TtAgo versus the RNA or DNA guide strands alone. Cumulative binding fraction plots are accompanied by the fluorescence intensity trace for a representative individual molecule. Red arrowheads, photobleaching of the Alexa555 guide; blue arrowheads, stepwise photobleaching of a single Alexa647 group; F, Förster resonance energy transfer from the Alexa555 guide to the Alexa647 target.

(B) Comparison of $k_{on}$ values for mouse AGO2-let-7a and TtAgo-let-7a. For let-7a and miR-21 RNA targets, mouse AGO2 and RNA alone values are reported as mean ± SD (n = 3), with >1,000 individual molecules collected. All other values were measured using several hundred individual molecules, and error of fit is reported.

See also Figures S2, S3, S4, and S5, Table S1, and Movies S1, S2, S3, and S4.

B

| Seed Sequence | Guide | Target | $k_{on}$ ($M^{-1}\cdot s^{-1}$) Guide alone | $k_{on}$ ($M^{-1}\cdot s^{-1}$) + AGO | |
|---|---|---|---|---|---|
| 5′-UGAGGUAGUAGGUUGUAUAGU-3′ | RNA | RNA | $9.1 \pm 1.7 \times 10^6$ | $3.9 \pm 0.5 \times 10^8$ | mouse AGO2 |
| 5′-UGAGGUAGUAGGUUGUAUAGU-3′ / UAGGUUGUAUAGU | RNA | RNA | $4.6 \pm 1.6 \times 10^6$ | $2.4 \pm 0.1 \times 10^8$ | |
| 5′-UGAGGUAGUAGGUUGUAUAGU-3′ / UAGG‖‖AUAGU | RNA | RNA | $5.1 \pm 1.8 \times 10^6$ | $2.8 \pm 0.5 \times 10^8$ | |
| 5′-UGAGGUAGUAGGUUGUAUAGU-3′ / AAAAAAAAA‖‖‖‖‖‖‖ | RNA | RNA | $7.6 \pm 0.9 \times 10^6$ | $3.6 \pm 0.2 \times 10^7$ | |
| 5′-UGAGGUAGUAGGUUGUAUAGU-3′ | RNA | DNA | $2.1 \pm 0.1 \times 10^6$ | $1.0 \pm 0.1 \times 10^9$ | |
| 5′-UGAGGUAGUAGGUUGUAUAGU-3′ / TAGGTTGUATAGT | RNA | DNA | | $7.8 \pm 0.2 \times 10^8$ | |
| 5′-UGAGGUAGUAGGUUGUAUAGU-3′ / TAGG‖‖‖ATAGT | RNA | DNA | | $6.4 \pm 0.2 \times 10^8$ | |
| 5′-UAGCUUAUCAGACUGAUGUUG-3′ | RNA | RNA | $5.3 \pm 0.2 \times 10^5$ | $1.3 \pm 0.1 \times 10^8$ | |
| 5′-TGAGGTAGTAGGTTGT-3′ | DNA | DNA | $4.7 \pm 0.1 \times 10^5$ | $6.4 \pm 0.1 \times 10^7$ | TtAgo |
| 5′-TGAGGTAGTAGGTTGT-3′ / TAGGTTGT | DNA | DNA | | $7.1 \pm 0.1 \times 10^7$ | |
| 5′-TGAGGTAGTAGGTTGT-3′ / TAGG‖‖‖ | DNA | DNA | | $4.8 \pm 0.1 \times 10^7$ | |
| 5′-TGAGGTAGTAGGTTGT-3′ | DNA | RNA | $4.6 \pm 0.1 \times 10^5$ | $6.2 \pm 0.1 \times 10^7$ | |
| 5′-TGAGGTAGTAGGTTGT-3′ / UAGGUUGU | DNA | RNA | | $2.0 \pm 0.1 \times 10^7$ | |
| 5′-TGAGGTAGTAGGTTGT-3′ / UAGG‖‖‖ | DNA | RNA | | $5.8 \pm 0.1 \times 10^6$ | |

values measured in ensemble binding experiments (Wee et al., 2012) or estimated by fitting pre-steady state ensemble data to a three-phase exponential model in which the fastest phase was assumed to correspond to $k_{on}$ (Deerberg et al., 2013).

To measure $k_{on}$ directly, we simultaneously recorded the fluorescence of individual target RNAs attached to the slide and individual molecules of fluorescent mouse AGO2-RISC (Figure 1D and Movies S1 and S2 and Supplemental Experimental Procedures). For each target molecule, RISC arrival was taken to be the first detectable co-localization of RISC and target. We readily detected RISC molecules that remained co-localized with target ≥ 200 ms (Supplemental Experimental Procedures). In Figure 1D, for example, when RISC arrives at ~40 s, the Alexa 555 fluorescence co-localizing with the Alexa647 target increases in a single step; it remains high until both Alexa555 (RISC) and Alexa647 (target) fluorescence drop to baseline at ~60 s, signifying target cleavage and simultaneous departure of RISC and the 3′ cleavage product. Figure 1E displays 426 individual single-molecule traces, ordered by time of target cleavage, as a "rastergram." Rastergrams summarize arrivals, departures, and target cleavage events for many individual target molecules.

To understand how AGO2 changes the rate at which an oligonucleotide arrives at a target, we compared $k_{on}$ of naked let-7a RNA and AGO2-bound let-7a (Figure 2). After arriving at the target, naked let-7a and AGO2-bound let-7a follow different paths. Formation of a 21 bp RNA:RNA duplex is essentially irreversible under physiological conditions, so observation of let-7a ended when its Alexa555 label photobleached. The target, labeled with 17 Alexa647 dyes, gradually lost fluorescence via discrete photobleaching events (Figure 2A and Movies S3 and S4). In contrast, binding of let-7a RISC ended with target cleavage; Alexa555 and Alexa647 signals were lost simultaneously.

On-rates ($k_{on}$) for RISC or let-7a alone were determined by fitting the cumulative distribution of arrivals to a single exponential, corrected for non-specific binding to the slide (Figure S1B and Supplemental Experimental Procedures). The $k_{on}$ of let-7a RNA alone hybridizing to a complementary target ($9.1 \pm 1.7 \times 10^6$ $M^{-1}\cdot s^{-1}$) was considerably slower than the rate of

macromolecular diffusion (Figures 2A and S2). let-7a comprises only A, G, and U nucleotides. Our measured $k_{on}$ for let-7a RNA agrees well with previous estimates for short oligonucleotides lacking G or C (Zhang et al., 2014). In comparison, $k_{on}$ for AGO2-bound let-7a, $3.9 \pm 0.5 \times 10^8$ $M^{-1} \cdot s^{-1}$, was ~43-fold faster than for let-7a alone (Figures 2A, S2, and S3). Thus, as proposed previously (Wee et al., 2012; Deerberg et al., 2013; Jung et al., 2013), Argonaute accelerates productive arrival of its guide at a complementary target sequence.

The unusual sequence composition of let-7a understates the general enhancement in target finding. Naked miR-21, which contains all four nucleotides, bound a complementary RNA target ~17 times more slowly than let-7a alone (Figures 2, S2, and S3). Mouse AGO2 accelerated miR-21 binding ~250-fold. We conclude that AGO2 generally accelerates target finding so that $k_{on}$ approaches the rate of macromolecular diffusion.

Acceleration of target finding is likely a general property of Argonaute proteins. We measured $k_{on}$ for TtAgo, the DNA-guided Argonaute protein (Swarts et al., 2014) from the eubacterium *Thermus thermophilus*. *T. thermophilus* grows at 62°C to 75°C (Cava et al., 2009), and TtAgo does not efficiently cleave either RNA or DNA at 37°C (Figure S4A). Control experiments established that the addition of an Alexa555 dye to the 3′ end of a DNA guide does not alter the ensemble binding properties of TtAgo (Figure S4B). In vivo, TtAgo binds 16 nt DNA guides (S.M.J. and P.D.Z., unpublished data), so we loaded TtAgo at 75°C with a single-stranded DNA corresponding to the first 16 nt of let-7a and then measured its binding at 37°C. The naked 16 nt let-7a guide bound a complementary RNA ~140 times more slowly ($k_{on} = 4.6 \pm 0.1 \times 10^5$ $M^{-1} \cdot s^{-1}$) than the same TtAgo-bound DNA guide ($k_{on} = 6.2 \pm 0.1 \times 10^7$ $M^{-1} \cdot s^{-1}$; Figures 2 and S4C).

Why is $k_{on}$ for TtAgo ~6 times slower than for AGO2? We suspect that, at 37°C, TtAgo spends less time in a binding-competent conformation, which is consistent with its greater cleavage activity at 75°C (Figure S4A). We conclude that both mouse AGO2 and TtAgo alter $k_{on}$, the rate-determining step for nucleic acid hybridization, ensuring that the speed at which Argonaute finds a complementary target RNA or DNA is limited by the rate of macromolecular diffusion.

## Argonaute Accelerates Target Finding by Creating the Seed Sequence

Argonaute proteins divide their guide RNAs into discrete functional domains. To determine which domain contributes most to the enhancement of target binding, we measured $k_{on}$ using (1) a target complementary just to the seed (g2–g8); (2) a target complementary to both the seed and the region of 3′ supplementary pairing (g13–g16); and (3) a target with complete complementarity to the guide (g2–g21; Figures 2B, S2, and S3). For each target RNA, we determined $k_{on}$ for the guide alone or loaded into AGO2 (Figures 2, S2, and S3). For a control RNA with ≤ 6 nt complementary to any region of the let-7a and ≤ 4 nt complementary to the let-7a seed, we were unable to detect any binding interactions above background binding to the slide (Figure S5A).

Structural comparisons of eubacterial and human AGO2 show that an N-terminal Argonaute domain prevents pairing beyond g16 in animal Argonautes; computational analyses of piRNAs in flies, silk moths, and mice suggest that target cleavage does not require complementarity beyond target position t16 (Wang et al., 2009b; Kwak and Tomari, 2012; Wee et al., 2012; Faehnle et al., 2013; Hauptmann et al., 2013; Wang et al., 2014). Thus, even targets with complete complementarity to a guide are unlikely to pair past g16 when bound to RISC.

In the absence of protein, nucleic acid hybridization is favored by greater complementarity, presumably because more potential base pairs provide more opportunities for nucleation, the rate-determining step for binding (Egli and Saenger, 1984). Consistent with this principle, $k_{on}$ of naked let-7a RNA increased ~2-fold between seed-only (g1–g8) or seed plus 3′ supplementary pairing (g1–g8 plus g13–g16) targets and the fully complementary target (g1–g21) (Figures 2B and S2). Yet when loaded in AGO2-RISC, let-7a bound all three targets with similar, near diffusion-limited on-rates (Figures 2B and S2). In contrast, the apparent rate of RISC finding an RNA fully complementary to let-7a except for the seed ($3.6 \pm 0.2 \times 10^7$ $M^{-1} \cdot s^{-1}$) was ~10-fold slower (Figures 2B and S5C). We observed similar $k_{on}$ effects for miR-21 RISC, whose $k_{on}$ was ~20-fold faster than miR-21 RNA alone when binding a target with complementarity only to the seed ($1.1 \pm 0.1 \times 10^7$ $M^{-1} \cdot s^{-1}$) or to both the seed and four, 3′ supplementary bases ($1.7 \pm 0.1 \times 10^7$ $M^{-1} \cdot s^{-1}$; Figure S2). We conclude that the seed sequence created by mouse AGO2 accounts for most of the enhancement in the rate of target finding.

To further test this idea, we measured $k_{on}$ for a series of six target RNAs bearing a dinucleotide mismatch in their seed-complementary sequence (Figures 3A, S3, and S5C). We performed these experiments at 10 frames $\cdot s^{-1}$, but $k_{on}$ values did not change at 25 frames $\cdot s^{-1}$ (data not shown). Compared to a seed-matched target, dinucleotide mismatches at guide positions g2g3, g3g4, g4g5, or g5g6 reduced $k_{on}$ 6.3- to 10-fold. Mismatches with positions g6g7 or g7g8 reduced $k_{on}$ just 1.3-fold, compared to a target complementary to the 7 nt seed. These data further suggest that Argonautes accelerate target finding by pre-organizing the seed and that acceleration is diminished when the seed pairing is disrupted at positions g2–g5.

TtAgo also required seed complementarity to accelerate target finding—$k_{on}$ for a DNA target complementary to the seed ($7.1 \pm 0.1 \times 10^7$ $M^{-1} \cdot s^{-1}$) or the seed and four, 3′ supplementary nucleotides ($4.8 \pm 0.1 \times 10^7$ $M^{-1} \cdot s^{-1}$) was essentially the same as when the entire target was complementary to the DNA guide ($6.4 \pm 0.1 \times 10^7$ $M^{-1} \cdot s^{-1}$; Figures 2 and S2 and Table S1).

A diffusion-limited bimolecular reaction is slower at higher viscosity (Berg and von Hippel, 1985). To test whether target finding by AGO2 similarly depends on viscosity, we measured $k_{on}$ for mouse let-7a-RISC in 0%, 20%—our standard conditions—or 50% glycerol (Figure S5B). As predicted for a diffusion-limited process, $k_{on}$ for a fully complementary target decreased with increasing viscosity: $6.4 \pm 0.1 \times 10^8$ $M^{-1} \cdot s^{-1}$ in 0%, $3.9 \pm 0.5 \times 10^8$ $M^{-1} \cdot s^{-1}$ in 20%, and $1.7 \pm 0.1 \times 10^8$ $M^{-1} \cdot s^{-1}$ in 50% glycerol.

## Seed Mismatches Cause Rapid Dissociation of Mouse AGO2 RISC

Ensemble experiments at 25°C show that mouse AGO2-RISC departs slowly from seed-matched targets ($\tau$ ~2,000 s at 25°C;

**A**

| Seed Sequence | $k_{on}$ ($M^{-1}s^{-1}$) Guide alone | $k_{on}$ ($M^{-1}s^{-1}$) + AGO | $k_{on}$ relative to seed |
|---|---|---|---|
| 5′-UGAGGUAGUAGGUUGUAUAGU-3′ | 4.6 ± 1.6 × $10^6$ | 2.4 ± 0.1 × $10^8$ | 1 |
| 5′-UGAGGUAGUAGGUUGUAUAGU-3′ | | 3.8 ± 0.1 × $10^7$ | 0.16 ± 0.01 |
| 5′-UGAGGUAGUAGGUUGUAUAGU-3′ | | 3.4 ± 0.2 × $10^7$ | 0.14 ± 0.01 |
| 5′-UGAGGUAGUAGGUUGUAUAGU-3′ | | 2.4 ± 0.1 × $10^7$ | 0.10 ± 0.01 |
| 5′-UGAGGUAGUAGGUUGUAUAGU-3′ | | 3.9 ± 0.1 × $10^7$ | 0.16 ± 0.01 |
| 5′-UGAGGUAGUAGGUUGUAUAGU-3′ | | 2.0 ± 0.1 × $10^8$ | 0.81 ± 0.03 |
| 5′-UGAGGUAGUAGGUUGUAUAGU-3′ | | 2.0 ± 0.1 × $10^8$ | 0.82 ± 0.03 |
| 5′-UGAGGUAGUAGGUUGUAUAGU-3′ | | 1.8 ± 0.1 × $10^8$ | 0.74 ± 0.02 |

**B**

| Seed Sequence | $k_{off}$ ($s^{-1}$) Guide alone (predicted) | $k_{off}$ ($s^{-1}$) + AGO (measured) | $k_{off}$ relative to seed | $K_D$ (nM) |
|---|---|---|---|---|
| 5′-UGAGGUAGUAGGUUGUAUAGU-3′ | 2.1 × $10^{-18}$ | N.D. | N.D. | N.D. |
| 5′-UGAGGUAGUAGGUUGUAUAGU-3′ | 8.5 × $10^{-5}$ | 0.0030 ± 0.0004 | 1.0 ± 0.1 | 0.011 ± 0.002 |
| 5′-UGAGGUAGUAGGUUGUAUAGU-3′ | 5.0 × $10^{-5}$ | 0.79 ± 0.08 | 220 ± 30 | 22 ± 3 |
| 5′-UGAGGUAGUAGGUUGUAUAGU-3′ | 0.094 | 0.0036 ± 0.0003 | 1 | 0.015 ± 0.002 |
| 5′-UGAGGUAGUAGGUUGUAUAGU-3′ | | 11 ± 1 | 3,000 ± 300 | 280 ± 40 |
| 5′-UGAGGUAGUAGGUUGUAUAGU-3′ | | 7.3 ± 0.5 | 2,000 ± 200 | 220 ± 30 |
| 5′-UGAGGUAGUAGGUUGUAUAGU-3′ | | 6.0 ± 0.4 | 1,700 ± 200 | 250 ± 40 |
| 5′-UGAGGUAGUAGGUUGUAUAGU-3′ | | 12 ± 1 | 3,200 ± 300 | 300 ± 40 |
| 5′-UGAGGUAGUAGGUUGUAUAGU-3′ | | 3.5 ± 0.1 | 960 ± 90 | 18 ± 2 |
| 5′-UGAGGUAGUAGGUUGUAUAGU-3′ | | 0.24 ± 0.01 | 67 ± 6 | 1.2 ± 0.2 |
| 5′-UGAGGUAGUAGGUUGUAUAGU-3′ | | 0.086 ± 0.002 | 24 ± 2 | 0.48 ± 0.06 |

**Figure 3. Role of the Seed Sequence in Target Binding**

Comparison of (A) $k_{on}$ and (B) $k_{off}$ of let-7a-guided mouse AGO2-RISC with different targets. Values were derived from data collected from several hundred individual RNA target molecules; error of fit is reported.

(A) $k_{on}$ values for let-7a-guided mouse AGO2-RISC to targets with complete seed-matched pairing or seed-matched pairing bearing dinucleotide mismatches.

(B) $k_{off}$ and *KD* values for nucleic acid in the absence of protein were predicted from the measured $k_{on}$ and ΔG37°C of binding calculated by nearest neighbor analysis (Reuter and Mathews, 2010; Turner and Mathews, 2010). $k_{off}$ was not determined for the fully complementary target because it was cleaved.

See also Figures S2, S3, S4, S5, and S6, Table S1, and Movies S1, S2, S3, and S4.

Wee et al., 2012), a timescale too long for direct observation of individual fluorescent molecules: photobleaching generally occurs before a departure is observed (Supplemental Experimental Procedures). As an alternative strategy to measure $k_{off}$ at 37°C, a more physiologically appropriate temperature, we measured apparent $k_{off}$ over a range of laser exposure and extrapolated to no exposure to obtain $k_{off}$: 0.0036 ± 0.0003 $s^{-1}$, ~280 s (Figure S5D). Photobleaching was much slower than dissociation for less complementary targets, so $k_{off}$ was readily measured by standard methods for targets containing a dinucleotide mismatch to the seed (Figures 3B, S3, and S6). RISC dissociated from these mismatched targets 70 to 3,200 times faster than a fully seed-matched target. As for $k_{on}$, g2–g6 base pairs within the seed contributed more to anchoring RISC on the target RNA than did base pairs to g7 or g8. A single-nucleotide mismatch to g8, converting a 7 nt seed to a 6 nt seed, increased $k_{off}$ 24-fold (Figures 3B and S3). Thus, AGO2 discriminates between seed-matched and seed-mismatched targets both during its initial search and once bound. RISC finds seed-mismatched targets more slowly and remains bound to them for less time than fully seed-complementary targets.

## Seed Pairing Explains AGO2 Binding to miRNA-like Targets

The effect of target:guide mismatches within the seed sequence cannot be accurately predicted from nearest-neighbor thermodynamic rules (Xia et al., 1998). For example, a dinucleotide mismatch at the end of a 7 nt seed-match is predicted to increase ΔG for RISC:target binding by 2.1–2.8 kcal·$mol^{-1}$ compared to a fully complementary seed match target site (g2–g8; Figure S6). In reality, the effect is much larger: a g2g3 dinucleotide mismatch (i.e., only g4–g8 paired) reduced the stability of the RISC:target complex by 6.1 ± 0.1 kcal·$mol^{-1}$, whereas a g7g8 mismatch (g2–g6 paired) reduced the stability of RISC binding by 2.7 ± 0.1 kcal·$mol^{-1}$ (Figure S6). However, a g3g4 mismatch, which is predicted to decrease binding stability by 6.1 kcal·$mol^{-1}$, reduced it by 5.9 ± 0.1 kcal·$mol^{-1}$.

Additional base pairs with the 3′ half of the guide (3′ supplementary pairing) are associated with high probability miRNA-binding sites (Grimson et al., 2007). The addition of four 3′ supplemental base pairs is predicted to change the $\Delta G_{37°C}$ of a fully base-paired let-7a seed by −3.7 kcal·$mol^{-1}$, yet our experiments failed to detect a substantial change in binding stability for let-7a bound to its target by seven seed base pairs or by seven seed plus four additional 3′ supplementary base pairs ($\Delta\Delta G_{37°C}$ = −0.20 ± 0.2 kcal·$mol^{-1}$). In contrast, dissociation of AGO2 guided by miR-21, which has a more AU-rich seed than *let-7*, was slowed >7-fold by adding 3′ supplementary base pairing (Figure S5E). Increasing the base-pairing strength of the seed by replacing three seed-match adenosines with 2,6 diaminopurine nucleotides decreased $k_{off}$ 4-fold and increased RISC affinity by –0.83 kcal·$mol^{-1}$, far less than the predicted –3 kcal·$mol^{-1}$ (Gryaznov and Schultz, 1994; Freier and Altmann, 1997).

## AGO2 Discriminates between RNA and DNA Targets

AGO2 has only been reported to regulate RNA targets. In contrast, only DNA targets have been identified in vivo for TtAgo (Wang et al., 2008a, 2008b; Wang et al., 2009b; Swarts et al., 2014). How do Argonaute proteins discriminate between RNA and DNA? We compared binding of AGO2 to RNA and DNA (Figures 2B and S2). As for RNA, AGO2 accelerated the target finding for DNA. In fact, $k_{on}$ for DNA was ~2.3–3.3 times faster than for RNA (Table S1). Yet AGO2-RISC did not remain stably bound to DNA, dissociating, on average, ~2.4 s after binding a seed-matched DNA target compared to ~280 s for RNA (Table S1 and Figures S3 and S5D). The >110-fold faster dissociation of AGO2 from DNA suggests that, even when acting in the nucleus, eukaryotic RISCs bind nascent transcripts, not single-stranded DNA (Bühler et al., 2006; Sabin et al., 2013).

Bacterial Argonautes are thought to target foreign DNA, such as horizontally transferred plasmids (Olovnikov et al., 2013; Swarts et al., 2014). Consistent with this function, TtAgo bound to and departed from RNA and DNA at similar rates (Figures 2B, S2, and S4C and Table S1).

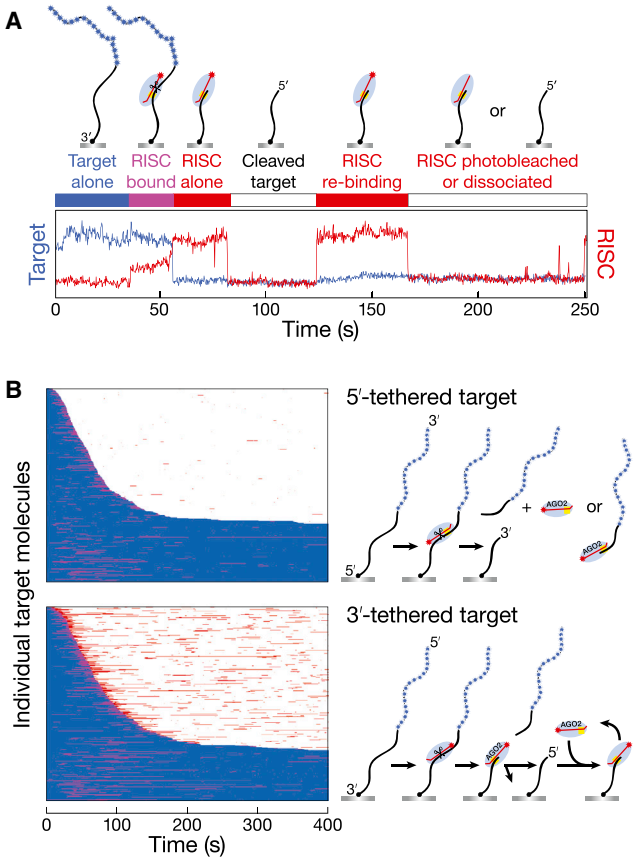


**Figure 4. let-7a Binds Tightly to the Seed-Matched, 3′ Product of Target Cleavage**

(A) A trace of an individual molecule of a 3′-tethered target fully complementary to let-7a. The trace shows that mouse let-7a-RISC bound the target (magenta bar), cleaved the target, and then remained bound to the 3′ product (red bar). Finally, RISC departed or the guide's Alexa555 photobleached. The 3′ cleavage product containing the seed remains on the slide surface, allowing a new molecule of RISC to bind.

(B) Rastergrams comparing 5′-tethered (426 individual molecules) and 3′-tethered (452 individual molecules) RNA targets fully complementary to let-7a.

## A Kinetic Framework for Mammalian RNAi

For a 5′-tethered target, cleavage by RISC leaves the 5′ product tethered to the slide surface, allowing detection only of RISC that remains bound via guide nucleotides g11–g21. For let-7a-guided AGO2, target cleavage and release of the 5′ product occurred simultaneously within the time resolution of our experiments (e.g., Figure 1D), suggesting that release of the 5′ product is faster than that of the seed-complementary 3′ product.

To measure 3′ product release, we synthesized a let-7a-complementary target with a 3′ biotin and 17 5′ Alexa647 dyes (Table S2). Using the 3′-tethered target, we detected four distinct reaction species: (1) target alone, (2) RISC bound to the target, (3) RISC bound to the 3′ cleavage product, and (4) the 3′ product after RISC dissociation (Figure 4A). Experiments with 5′-tethered target detected RISC bound to 5′ cleavage product and the 5′ product alone, completing the set of observable species in the RNAi reaction (Figure 4B).

As expected, the $k_{on}$ of let-7a-AGO2-RISC for a 3′-tethered target ($3.7 \pm 0.1 \times 10^8$ $M^{-1} \cdot s^{-1}$; data not shown) was nearly identical to $k_{on}$ for a 5′-tethered target ($3.9 \pm 0.5 \times 10^8$ $M^{-1} \cdot s^{-1}$; Figures 2B and S2). However, the order and rates of dissociation differed considerably for the 5′ and 3′ cleavage products (Figure 4B). The first product to be released was nearly always the 5′ product, after which RISC slowly dissociated from the 3′ product. The 3′ product is complementary to the seed sequence, and after RISC departed, we frequently observed additional RISC binding events to the tethered product (Figure 4B).

To quantitatively assess product release, we fit our data (Figure 5A) to a unified reaction scheme that accounts for all observed intermediates and products (Figure 5B). A global fit is possible for our kinetic data because the loss or production of different reaction species (e.g., 5′- and 3′-products) shares one or more kinetic steps in the mechanism. By fitting multiple datasets simultaneously to the same kinetic mechanism, the rate constants for shared steps become global parameters constrained to be the same for all datasets. Our proposed reaction mechanism includes branched pathways for product release: one branch corresponds to 5′ product release followed by 3′ product released (Figure 5B, $k_{5'\ 1st}$ followed by $k_{3'\ 2nd}$), whereas in the other, the order of product release is reversed (Figure 5B, $k_{3'\ 1st}$ followed by $k_{5'\ 2nd}$). Both branches achieve the same final state: two free products and free AGO2-RISC.

Accounting for the sigmoidal kinetics of product release (Figure 5A) required an additional kinetic step that was shared by both branches; its rate constant ($k$) was treated as a global parameter for fitting. $k$ likely corresponds to the rate of the slowest step in target cleavage, probably the change in Argonaute conformation that brings the catalytic $Mg^{2+}$ near the scissile phosphate (Wang et al., 2009b; Sheng et al., 2014). The global fit based on four experimentally measured product release curves obtained using 5′- and 3′-tethered targets (Figures S7A and S7B) defined three of the five rate constants ($k$, $k_{5'\ 1st}$, and $k_{3'\ 1st}$). The rate constants ($k_{3'\ 2nd}$ and $k_{5'\ 2nd}$) for release of the 3′ or 5′ products following release of the other product were determined directly from the distributions of waiting times beginning with the departure of the first cleavage product and ending with the departure of the second (Figures S7A and S7B), after subtracting the photobleaching rate.

## Seed Pairing Determines the Rate of Slicing and the Order of Product Release

To determine whether the features of cleavage and product release observed for let-7a RISC depend on guide RNA sequence, we performed parallel experiments with let-7a-RISC and a 5′-tethered let-7a target with t4t5 mismatches to the seed (Figures S3 and S5C) and with miR-21-RISC and 5′- and 3′-tethered miR-21 targets. Global fitting of these data to our kinetic scheme (Figures 5B and S7A) gave the slicing and product release rates and order.

Slicing rate depended on guide strand identity—let-7a had the slowest slicing rate we measured ($k$ = 0.15 $s^{-1}$); miR-21-RISC cleaved its target twice as fast ($k$ = 0.31 $s^{-1}$). The let-7a seed has stronger predicted base pairing ($\Delta G$ = −15.6 kcal·$mol^{-1}$) than miR-21 ($\Delta G$ = −13.3 kcal·$mol^{-1}$). The let-7a target with seed mismatches had the weakest predicted

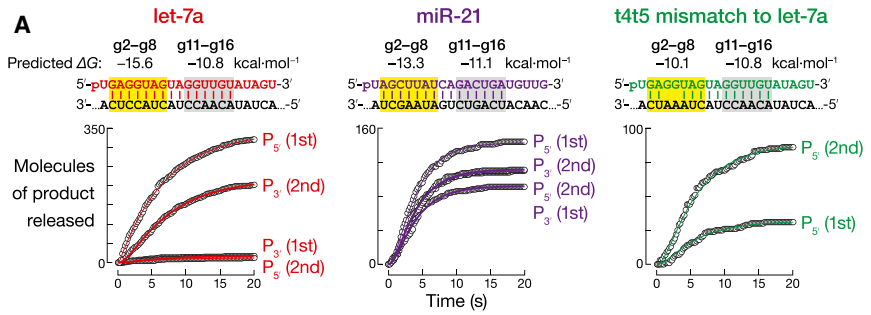


**Figure 5. AGO2-Catalyzed Cleavage and Product Release**

(A) Global fit analysis (Supplemental Experimental Procedures) of 5′- and 3′-tethered targets for AGO2 guided by let-7a or miR-21.

(B) The detailed kinetic scheme used for global fitting. Rate constants are color coded according to (A). Percentages in parentheses report the proportion of product molecules released first.

See also Figure S7.

seed base pairing (ΔG = −10.1 kcal·mol$^{-1}$) and cleaved faster than the fully complementary let-7a target ($k = 0.20\ s^{-1}$) but slower than miR-21. Our data suggest that efficient target cleavage requires seed pairing that is neither too strong nor too weak.

The relative base-pairing stability of the seed and 3′ half of the guide determines the order of product release, as evidenced by the proportion of the reaction directed through each of the two product-release branches (Figure 5B). For let-7a, whose seed is predicted to pair more stably than its 3′ half, the 5′ product departed first for 92% of target molecules; release of the 3′ cleavage product limited the rate of enzyme turnover, $k_{cat}$. For the let-7a target with t4t5 mismatches, the 3′ product left before the 5′ for 74% of molecules. In contrast, the seed and 3′ half of miR-21 have similar base pairing stabilities, and 57% of the 5′ product departed first. We conclude that the order of product release reflects the sequence of the guide and target, following no set order.

## Release of the First Product Promotes Release of the Second

Formally, there are two rates for the release of each cleavage product: a rate for when the product departs first and a rate for when the same product departs second, the other product having already dissociated. For example, $k_{5'\ 1st}$ is the rate for 5′ product release in the presence of bound 3′ product, whereas $k_{5'\ 2nd}$ is the rate for 5′ product release after the 3′ product has left. Our data suggest that release of the first product promotes release of the second product (Figure 5). For example, the 5′ and 3′ product rates for miR-21 were both ~4-fold faster when the products were released second rather than first. Similarly, release of the 5′ product of the let-7a seed-mismatched target was 0.21 ± 0.01 s$^{-1}$ when released first but 1.3 ± 0.1 s$^{-1}$ when released second. A notable exception was the seed-matched 3′ product of let-7a target, by far the most stably bound product we examined. This 3′ cleavage product dissociated at ~0.05 s$^{-1}$ regardless of the presence of the 5′ product.

We can imagine two mechanisms by which departure of one product can accelerate dissociation of the other: (1) binding may be mutually stabilized by stacking interactions between the terminal bases of the two products, or (2) departure of one product may facilitate a conformational change that destabilizes the second. Such a conformational change might correspond to the return of the endonuclease active site to the conformation present prior to zippering of the guide:target helix 3′ to the seed sequence (Wang et al., 2009b; Elkayam et al., 2012; Schirle and MacRae, 2012; Faehnle et al., 2013).

## Strong Seed Pairing Slows RISC Turnover

The rates for target cleavage and product release allow calculation of the overall turnover rate: $k_{cat} = k \cdot k_{5'\ 1st} \cdot k_{3'\ 2nd} / (k \cdot k_{5'\ 1st} + k \cdot k_{3'\ 2nd} + k_{5'\ 1st} \cdot k_{3'\ 2nd})$ when the 5′ product is released first, and $k_{cat} = k \cdot k_{3'\ 1st} \cdot k_{5'\ 2nd} / (k \cdot k_{3'\ 1st} + k \cdot k_{5'\ 2nd} + k_{3'\ 1st} \cdot k_{5'\ 2nd})$ when the 3′ product is released first. As expected, the two pathways have similar $k_{cat}$ values. For let-7a, the calculated $k_{cat}$ value, 0.036 ± 0.002 s$^{-1}$, agrees well with $k_{cat}$ determined by ensemble analysis (0.066 ± 0.004 s$^{-1}$; Figure 1C). The turnover rate was ~4-fold faster for both miR-21 (0.16 ± 0.1 s$^{-1}$) and let-7a with the g4g5 seed-mismatched target (0.13 ± 0.1 s$^{-1}$). The slower $k_{cat}$ for let-7a reflects the stronger seed pairing to its fully complementary target; the slow 3′ product release step limits overall turnover. Both miR-21, with its weaker pairing strength in its seed, and let-7a, with intentionally weakened seed pairing to a target with g4g5 mismatches, direct faster cleavage than let-7a with a fully complementary target; their product release rates are comparable to or faster than $k$, the apparent RISC cleavage rate (Figure 5B). Thus, siRNAs with more stable base pairing between seed and target are predicted to cleave fewer targets per unit time than targets whose rate of 3′ product release is not rate determining.

The autoantigen protein La has been proposed to facilitate multiple-turnover target cleavage by human AGO2 by accelerating product release (Liu et al., 2011). To test this idea, we measured the rate of multiple-turnover target cleavage by let-7a RISC in the absence or presence of equimolar (1 nM) or excess (50 or 500 nM) La protein (Figure S7C). We were unable to detect any increase in target cleavage rate in the

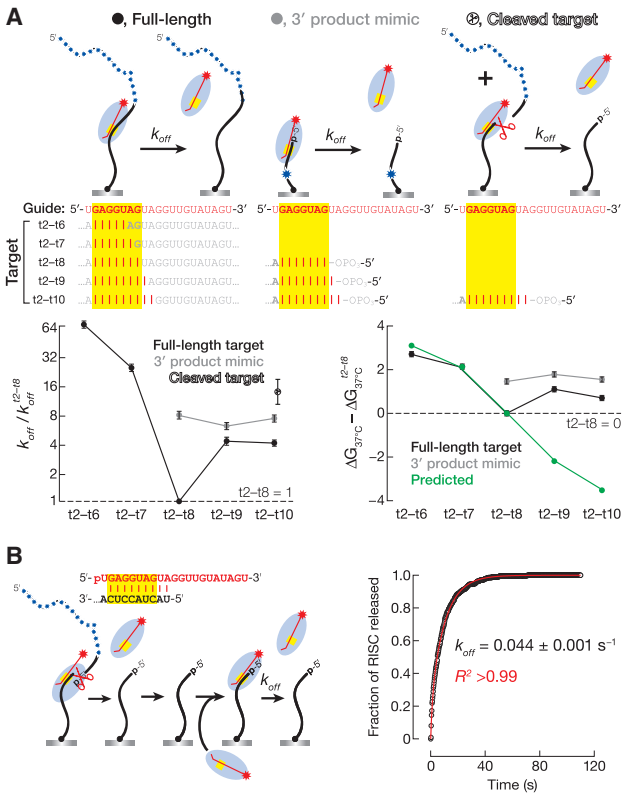


**Figure 6. Argonaute Can Distinguish between miRNA Targets and Cleaved Products**

(A) Effects of additional complementarity and 3′ target length on RISC binding and dissociation. $k_{off}$ was measured directly, correcting for photobleaching, except for the seed-matched, full-length target, whose dissociation was slower than the rate of photobleaching and was therefore measured by varying laser exposure time and extrapolating to no illumination. $\Delta\Delta G_{37°C}$ was calculated from $K_D$ ( = $k_{off}$ / $k_{on}$); theoretical $\Delta\Delta G_{37°C}$ was predicted using nearest-neighbor analysis to estimate $\Delta G$.

(B) Experimentally measured $k_{off}$, corrected for photobleaching, for let-7a-guided mouse AGO2-RISC dissociating from the 3′ product of a previously cleaved, 3′-tethered, fully complementary target RNA.

See also Figures S5, S6, and S7.

presence of La. We conclude that, in cells, La protein is unlikely to overcome the rate-limiting step of product release for let-7a RISC.

## AGO2 Distinguishes between miRNA-like Binding Sites and Cleavage Products

Although quantitatively different from the energetics of nucleic acid hybridization, the free energy of base pairing between a seed sequence and its target influences the rates of all steps in the RNAi reaction, including binding and dissociation of RISC, cleavage of the target, and release of the cleaved products. However, one aspect of RISC function emerges from our studies that is not predicted by the stability of guide-target base pairing: AGO2 appears to discriminate between a miRNA-like binding site, which typically pairs only with nucleotides g2–g8, and binding to the seed-matched, 3′ product of target cleavage, which pairs with nucleotides g2–g10 (Figure 6).

We measured the $k_{off}$ for let-7a-AGO2-RISC bound to targets complementary to g2–g8 (seed), g2–g9, or g2–g10, as would be found for a 3′ cleavage product. The standard rules for nucleic acid hybridization predict that the addition of one or two additional base pairs beyond the seed should slow dissociation of RISC (Figure 6). Counterintuitively, additional base pairs increased dissociation ~4-fold: $k_{off}$ was 0.014 ± 0.001 s$^{-1}$ when g2–g9 paired with the target and 0.015 ± 0.001 s$^{-1}$ (τ ~66 s) when g2–g10 paired but 0.0036 s$^{-1}$ (τ ~280 s) when only g2–g8 were paired. In vivo, miRNAs have little opportunity to bind targets t2–t10 complementarity, but this pairing scheme is typically found in the 3′ cleavage product generated by the RNAi pathway. In fact, RISC departed >3-fold faster from the 3′ product generated by target cleavage ($k_{off}$ = 0.05 ± 0.01 s$^{-1}$), which ends after t10, than the corresponding full-length target and ~14-fold faster than from the full-length, seed-matched (t2–t8) target. When the 3′ cleavage product was subsequently bound by other RISC molecules, they depart at essentially the same rate as the RISC that first catalyzed cleavage, $k_{off}$ = 0.044 ± 0.001 s$^{-1}$ (τ ~23 s; Figure 6B).

One potential explanation for the accelerated departure of RISC from a 3′ cleavage product compared to a full-length, seed-matched target is that the full-length target extends far beyond position t10, providing opportunities for non-sequence-specific interactions between AGO2 and its target. To test this idea, we designed a series of 5′ monophosphorylated, 30 nt RNAs that end at either position t8, t9, or t10 (Figure 6A). RISC dissociated nearly twice as fast from the 3′ cleavage product mimic complementary to g2–g10 as from the corresponding full-length target (Figure 6). RISC departed ~8-fold faster from a seed-matched 3′ cleavage product mimic than from a seed-matched, full-length target. These data reinforce the idea that AGO2 makes sequence-independent contacts with its RNA targets (Ameres et al., 2007).

Nonetheless, such contacts do not explain why RISC departed faster when paired with t2–t9 or t2–t10 than with t2–t8. How does g9:t9 pairing alter the properties of RISC so that it binds more weakly to an RNA with eight or nine potential base pairs than to an RNA with which it makes only seven? Extending base pairing beyond position g8 of the seed may require opening the central cleft of AGO2, a presumably unfavorable conformational change (Schirle et al., 2014). These properties of AGO2 were not anticipated from thermodynamic predictions for the strength of nucleic acid base pairing (Figures 6 and S6).

## DISCUSSION

Argonaute proteins from both bacteria and mammals accelerate the rate at which their guides find complementary targets. Argonaute can accelerate the on-rate as much as 250-fold, and DNA-guided TtAgo and mouse RNA-guided AGO2 both enhance target finding for DNA and RNA targets. The acceleration of target binding by AGO2 requires seed complementarity with its target, which is consistent with pre-organization of the seed sequence playing a major role in this phenomenon. However, seed nucleotides do not contribute equally to target binding; g2–g5 base pairs contribute more to the initial binding of RISC to target RNA than g6–g8 base pairs, which function

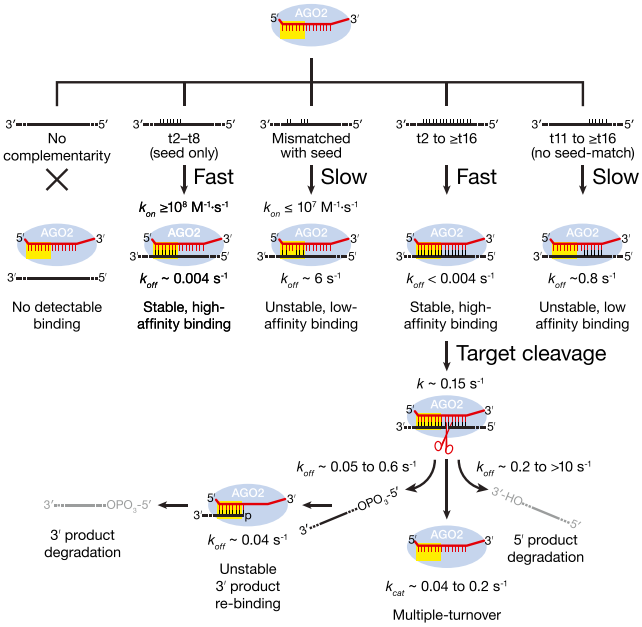


**Figure 7. A Kinetic Model for Mouse AGO2-RISC Function**

mainly to slow dissociation of RISC after a successful encounter with target. The existence of seed subdomains with distinct binding functions was first predicted from the structure of human AGO2-RISC bound to a seed-matched RNA (Schirle et al., 2014).

Because target binding is bimolecular, the rate at which RISC acquires targets in vivo reflects the concentrations of both target sites and RISC. In light of recent reports that in vivo target site concentration is both high and exceeds that of miRNA-guided RISC (Denzler et al., 2014), the rate of target finding is unlikely to limit the speed at which miRNAs destabilize their target mRNAs. In fact, the rates of target binding reported here approach the speed of macromolecular diffusion, suggesting that additional proteins such as poly(A) binding protein cannot promote association of RISC with seed-complementary targets, as has been suggested (Moretti et al., 2012). Of course, our studies were conducted with purified components outside of the cell, and future experiments measuring the rates of RISC diffusion, and target binding in living cells will be needed to test these ideas.

In addition to accelerating binding of guides to targets, Argonaute proteins alter how quickly target sequences dissociate from RISC. For mouse AGO2 at 37°C, RISC remains bound to a typical miRNA-binding site for ~5 min. In fact, many miRNA-guided Argonautes are predicted to bind their target sites with greater affinity than most known RNA-binding proteins. Consequently, RISC likely serves to recruit and stabilize binding of proteins such as GW182 or mRNA-degrading nucleases. The high binding affinity of RISC reflects its slow dissociation rate, which is far slower than expected for seven base pairs between RNA strands; the $K_D$ of a guide RNA in RISC bound to a seed-match target is ~19,000 times tighter and dissociates ~360 times slower than for RNA alone.

Many of these properties spring from the unique configuration of guide nucleotides g2–g8 within Argonaute proteins. Our data show that the sequence of the seed influences the rate of dissociation, with RISC dissociating from a seed-matched target far more slowly when guided by let-7a than by miR-21. Moreover, mismatches in the seed increase the dissociation of RISC more than would be predicted from the thermodynamics of base pairing (Figure S6). For example, a g2g3 mismatch increased $k_{off}$ ~3,000-fold, an ~6 kcal·$mol^{-1}$ increase in free energy; for RNAs hybridizing in the absence of protein, the predicted change is just −3 kcal·$mol^{-1}$. Together, our data suggest that Argonautes do more than simply pre-organize the seed, which would pre-pay the entropic cost of hybridization to a similar extent for all seed sequences (Figure 7). Argonaute proteins must also provide an environment in which the free energy of each non-seed base pair is decreased, but the rank order of base-pairing strength predicted by nearest-neighbor analysis remains essentially unchanged. Guide positions g9 and g10 are a notable exception to this idea: complementarity to t9 and t10 can actively destabilize RISC binding. Thus, miRNA prediction algorithms that penalize or at least give no credit for pairing at nucleotides t9 and t10 are more likely to identify biologically important mRNA targets.

Intriguingly, mismatches at the 5′ end of the seed have the greatest effect on $k_{off}$ (Figure 3), even when these mismatches are not predicted to have the greatest effect on base pairing stability (Figure S6). Thus, even within the seed sequence, Argonaute assigns greater value to mismatches before position g5 than from g5–g8. Pairing of g2–g5 with a target appears to be "all or none," with both central and terminal dinucleotide mismatches disrupting binding to a similar extent (Figure S6). Nucleotides g6–g8 form a second subdomain, and mismatches in this region increase $k_{off}$ to a far smaller extent. Notably, the structure of human AGO2-RISC bound to a seed-matched target suggests that pairing beyond g5 requires a conformational rearrangement in the protein (Schirle et al., 2014).

Although most miRNA-binding sites match the seed sequence, some sites use centered pairing, ≥ 11 nt of contiguous complementarity typically starting at position t4 (Shin et al., 2010). Although target mismatches with the 5′ end of the seed normally prevent stable miRNA binding, extensive complementarity to the center and 3′ end of a miRNA may compensate. Supporting this idea, let-7a-RISC binding to a seed-matched target containing a g4g5:t4t5 mismatch was rescued by additional base pairs 3′ to the seed (Figures 3 and S5). In vivo, miR-21 binds *Glutathione S-transferase Mu 3* mRNA by pairing with nucleotides t5–t16 (Shin et al., 2010). We speculate that the faster-than-typical $k_{off}$ of the miR-21 seed (Figures 3 and S5) facilitated the evolution of this site. Because centered sites extend well into the 3′ region of the guide, centered pairing may offset the destabilizing effects of g9g10 complementarity. Alternatively, the absence of g2–g4 seed pairing may alleviate the conformational strain associated with g2–g10 complementarity.

The extent of complementarity between guide and target determines whether RISC simply binds or binds and cleaves. In animals, miRNAs typically guide binding, whereas siRNAs usually direct target cleavage. Our data suggest that mammalian AGO2 can discriminate between seed-matched "miRNA

targets," to which RISC remains tightly bound, and "siRNA targets," with which it pairs more extensively. After target cleavage, release of the two cleavage products follows no strict order. AGO2 creates an environment in which dissociation of either of the cleavage products accelerates departure of the other product. Release of either cleavage product can be rate determining but is nevertheless faster than would be predicted from the extent of base pairing with the guide. For the 3′ product, faster-than-expected release can be explained, in part, by the loss of non-sequence-specific protein-RNA contacts after the 5′ product leaves.

TtAgo also senses the type of target to which it is bound. In vivo, TtAgo catalyzes cleavage of foreign DNA with extensive complementarity to its 16 nt DNA guide (S.M.J. and P.D.Z., unpublished data; Swarts et al., 2014). Consistent with this idea, TtAgo dissociated slowly from a fully complementary target DNA but quickly from a target that was only partially complementary ($\tau \leq 1$ s at 37°C; Table S1). Unlike mouse AGO2, which appears to have evolved to bind stably only to RNA, TtAgo readily binds and cleaves both DNA and RNA. In contrast, mouse AGO2 finds complementary sites in DNA more rapidly than RNA but quickly leaves DNA ($\tau \leq 2$ s; Table S1). RNA-guided human AGO2, but not DNA-guided TtAgo, makes sequence-independent contacts with both the guide and the target in the minor groove of the helix formed by seed:target pairing (Wang et al., 2008a; Schirle et al., 2014). The absence of minor groove contacts may explain why TtAgo-RISC departs more rapidly from partially complementary targets than does human AGO2-RISC.

Unlike ensemble approaches, single-molecule studies allow direct and continuous observation of rapid events for both the target and guide. We anticipate that future studies will extend this approach to other Argonaute proteins, including the animal-specific PIWI clade, which defends the germline against transposons, and plant Argonautes, which mediate both mRNA cleavage (Llave et al., 2002; Tang et al., 2003) and repression of mRNA translation (Brodersen et al., 2008; Iwakawa and Tomari, 2013), as well as to more complex sets of proteins that collaborate with Argonautes to repress gene expression.

## EXPERIMENTAL PROCEDURES

### RISC Purification

A duplex siRNA with a 3′ Alexa Fluor 555 (Life Technologies) labeled guide strand was incubated in S100 extract from *Ago2*$^{-/-}$ mouse embryonic fibroblasts overexpressing mouse AGO2 (O'Carroll et al., 2007), and RISC purified as described (Flores-Jasso et al., 2013). TtAgo was assembled with a 16 nt, 3′ Alexa Fluor 555-labeled single-stranded DNA guide.

### Single-Molecule Spectroscopy and Data Analysis

Images were collected using a IX81-ZDC2 zero-drift, inverted microscope (Olympus) equipped with a motorized, multicolor TIRF illuminator, 100W lasers, and a 100× high numerical aperture objective maintained at 37°C. Images were recorded with two EM-CCD cameras (ImagEM, Hamamatsu Photonics) using a dichroic image splitter (DC2, Photometrics) to separate fluorescent emission from the two spectrally distinct fluorescent dyes. Acquisition parameters were controlled with Metamorph software (Molecular Devices), and image analysis was performed in MATLAB using custom scripts and a co-localization analysis package developed by the Gelles laboratory (Friedman and Gelles, 2015). Location of Alexa 647 target molecules (red channel) and mapping of target locations to the Alexa 555 guide molecules (green channel) were as described (Crocker and Grier, 1996; Friedman et al., 2013). On- and off-rates were corrected for non-specific binding to the slide surface; all dissociation rates were corrected for photobleaching. Global fitting to a unified kinetic scheme was performed in DynaFit 4 (BioKin; Kuzmic, 1996).

## SUPPLEMENTAL INFORMATION

Supplemental Information includes Supplemental Experimental Procedures, seven figures, two tables, and four movies and can be found with this article online at http://dx.doi.org/10.1016/j.cell.2015.06.029.

## ACKNOWLEDGMENTS

We thank members of the M.J.M. and P.D.Z. laboratories for discussions and comments on the manuscript; Jeff Gelles and Larry Friedman for experimental and analytical advice; and Johnson Chung for scripts to create overlay movies. This work was supported in part by NIH grants GM053007 and GM053007 to M.J.M. and GM62862 and GM65236 to P.D.Z.

Received: December 3, 2014
Revised: April 1, 2015
Accepted: June 9, 2015
Published: July 2, 2015; corrected online July 8, 2016

## REFERENCES

Ameres, S.L., Martinez, J., and Schroeder, R. (2007). Molecular basis for target RNA recognition and cleavage by human RISC. Cell *130*, 101–112.

Berg, O.G., and von Hippel, P.H. (1985). Diffusion-controlled macromolecular interactions. Annu. Rev. Biophys. Biophys. Chem. *14*, 131–160.

Brodersen, P., Sakvarelidze-Achard, L., Bruun-Rasmussen, M., Dunoyer, P., Yamamoto, Y.Y., Sieburth, L., and Voinnet, O. (2008). Widespread translational inhibition by plant miRNAs and siRNAs. Science *320*, 1185–1190.

Bühler, M., Verdel, A., and Moazed, D. (2006). Tethering RITS to a nascent transcript initiates RNAi- and heterochromatin-dependent gene silencing. Cell *125*, 873–886.

Cava, F., Hidalgo, A., and Berenguer, J. (2009). *Thermus thermophilus* as biological model. Extremophiles *13*, 213–231.

Crocker, J.C., and Grier, D.G. (1996). Methods of digital video microscopy for colloidal studies. J. Colloid Interface Sci. *179*, 298–310.

Deerberg, A., Willkomm, S., and Restle, T. (2013). Minimal mechanistic model of siRNA-dependent target RNA slicing by recombinant human Argonaute 2 protein. Proc. Natl. Acad. Sci. USA *110*, 17850–17855.

Denzler, R., Agarwal, V., Stefano, J., Bartel, D.P., and Stoffel, M. (2014). Assessing the ceRNA hypothesis with quantitative measurements of miRNA and target abundance. Mol. Cell *54*, 766–776.

Egli, M., and Saenger, W. (1984). Principles of Nucleic Acid Structure (Springer-Verlag).

Elbashir, S.M., Lendeckel, W., and Tuschl, T. (2001a). RNA interference is mediated by 21- and 22-nucleotide RNAs. Genes Dev. *15*, 188–200.

Elbashir, S.M., Martinez, J., Patkaniowska, A., Lendeckel, W., and Tuschl, T. (2001b). Functional anatomy of siRNAs for mediating efficient RNAi in *Drosophila melanogaster* embryo lysate. EMBO J. *20*, 6877–6888.

Elkayam, E., Kuhn, C.D., Tocilj, A., Haase, A.D., Greene, E.M., Hannon, G.J., and Joshua-Tor, L. (2012). The structure of human argonaute-2 in complex with miR-20a. Cell *150*, 100–110.

Faehnle, C.R., Elkayam, E., Haase, A.D., Hannon, G.J., and Joshua-Tor, L. (2013). The making of a slicer: activation of human Argonaute-1. Cell Rep. *3*, 1901–1909.

Flores-Jasso, C.F., Salomon, W.E., and Zamore, P.D. (2013). Rapid and specific purification of Argonaute-small RNA complexes from crude cell lysates. RNA *19*, 271–279.

Freier, S.M., and Altmann, K.H. (1997). The ups and downs of nucleic acid duplex stability: structure-stability studies on chemically-modified DNA:RNA duplexes. Nucleic Acids Res. *25*, 4429–4443.

Friedman, L.J., and Gelles, J. (2015). Multi-wavelength single-molecule fluorescence analysis of transcription mechanisms. Methods. Published online May 30, 2015. http://dx.doi.org/10.1016/j.ymeth.2015.05.026.

Friedman, L.J., Chung, J., and Gelles, J. (2006). Viewing dynamic assembly of molecular complexes by multi-wavelength single-molecule fluorescence. Biophys. J. *91*, 1023–1031.

Friedman, L.J., Mumm, J.P., and Gelles, J. (2013). RNA polymerase approaches its promoter without long-range sliding along DNA. Proc. Natl. Acad. Sci. USA *110*, 9740–9745.

Grimson, A., Farh, K.K., Johnston, W.K., Garrett-Engele, P., Lim, L.P., and Bartel, D.P. (2007). MicroRNA targeting specificity in mammals: determinants beyond seed pairing. Mol. Cell *27*, 91–105.

Gryaznov, S., and Schultz, R.G. (1994). Stabilization of DNA:DNA and DNA/RNA duplexes by substitution of 2′-deoxyadenosine with 2′-deoxy-2-aminoadenosine. Tetrahedron Lett. *35*, 2489–2492.

Haley, B., and Zamore, P.D. (2004). Kinetic analysis of the RNAi enzyme complex. Nat. Struct. Mol. Biol. *11*, 599–606.

Hauptmann, J., Dueck, A., Harlander, S., Pfaff, J., Merkl, R., and Meister, G. (2013). Turning catalytically inactive human Argonaute proteins into active slicer enzymes. Nat. Struct. Mol. Biol. *20*, 814–817.

Herschlag, D. (1991). Implications of ribozyme kinetics for targeting the cleavage of specific RNA molecules in vivo: more isn't always better. Proc. Natl. Acad. Sci. USA *88*, 6921–6925.

Huntzinger, E., and Izaurralde, E. (2011). Gene silencing by microRNAs: contributions of translational repression and mRNA decay. Nat. Rev. Genet. *12*, 99–110.

Iwakawa, H.O., and Tomari, Y. (2013). Molecular insights into microRNA-mediated translational repression in plants. Mol. Cell *52*, 591–601.

Jung, S.R., Kim, E., Hwang, W., Shin, S., Song, J.J., and Hohng, S. (2013). Dynamic anchoring of the 3′-end of the guide strand controls the target dissociation of Argonaute-guide complex. J. Am. Chem. Soc. *135*, 16865–16871.

Krek, A., Grün, D., Poy, M.N., Wolf, R., Rosenberg, L., Epstein, E.J., MacMenamin, P., da Piedade, I., Gunsalus, K.C., Stoffel, M., and Rajewsky, N. (2005). Combinatorial microRNA target predictions. Nat. Genet. *37*, 495–500.

Kuzmic, P. (1996). Program DYNAFIT for the analysis of enzyme kinetic data: application to HIV proteinase. Anal. Biochem. *237*, 260–273.

Kwak, P.B., and Tomari, Y. (2012). The N domain of Argonaute drives duplex unwinding during RISC assembly. Nat. Struct. Mol. Biol. *19*, 145–151.

Lewis, B.P., Shih, I.H., Jones-Rhoades, M.W., Bartel, D.P., and Burge, C.B. (2003). Prediction of mammalian microRNA targets. Cell *115*, 787–798.

Lewis, B.P., Burge, C.B., and Bartel, D.P. (2005). Conserved seed pairing, often flanked by adenosines, indicates that thousands of human genes are microRNA targets. Cell *120*, 15–20.

Lim, L.P., Lau, N.C., Garrett-Engele, P., Grimson, A., Schelter, J.M., Castle, J., Bartel, D.P., Linsley, P.S., and Johnson, J.M. (2005). Microarray analysis shows that some microRNAs downregulate large numbers of target mRNAs. Nature *433*, 769–773.

Lingel, A., Simon, B., Izaurralde, E., and Sattler, M. (2004). Nucleic acid 3′-end recognition by the Argonaute2 PAZ domain. Nat. Struct. Mol. Biol. *11*, 576–577.

Liu, J., Carmell, M.A., Rivas, F.V., Marsden, C.G., Thomson, J.M., Song, J.J., Hammond, S.M., Joshua-Tor, L., and Hannon, G.J. (2004). Argonaute2 is the catalytic engine of mammalian RNAi. Science *305*, 1437–1441.

Liu, Y., Tan, H., Tian, H., Liang, C., Chen, S., and Liu, Q. (2011). Autoantigen La promotes efficient RNAi, antiviral response, and transposon silencing by facilitating multiple-turnover RISC catalysis. Mol. Cell *44*, 502–508.

Llave, C., Xie, Z., Kasschau, K.D., and Carrington, J.C. (2002). Cleavage of *Scarecrow-like* mRNA targets directed by a class of *Arabidopsis* miRNA. Science *297*, 2053–2056.

Ma, J.B., Ye, K., and Patel, D.J. (2004). Structural basis for overhang-specific small interfering RNA recognition by the PAZ domain. Nature *429*, 318–322.

Martinez, J., and Tuschl, T. (2004). RISC is a 5′ phosphomonoester-producing RNA endonuclease. Genes Dev. *18*, 975–980.

Moretti, F., Kaiser, C., Zdanowicz-Specht, A., and Hentze, M.W. (2012). PABP and the poly(A) tail augment microRNA repression by facilitated miRISC binding. Nat. Struct. Mol. Biol. *19*, 603–608.

Nakanishi, K., Weinberg, D.E., Bartel, D.P., and Patel, D.J. (2012). Structure of yeast Argonaute with guide RNA. Nature *486*, 368–374.

Nygaard, A.P., and Hall, B.D. (1964). Formation and properties of RNA-DNA complexes. J. Mol. Biol. *9*, 125–142.

O'Carroll, D., Mecklenbrauker, I., Das, P.P., Santana, A., Koenig, U., Enright, A.J., Miska, E.A., and Tarakhovsky, A. (2007). A Slicer-independent role for Argonaute 2 in hematopoiesis and the microRNA pathway. Genes Dev. *21*, 1999–2004.

Olovnikov, I., Chan, K., Sachidanandam, R., Newman, D.K., and Aravin, A.A. (2013). Bacterial argonaute samples the transcriptome to identify foreign DNA. Mol. Cell *51*, 594–605.

Parker, J.S., Roe, S.M., and Barford, D. (2005). Structural insights into mRNA recognition from a PIWI domain-siRNA guide complex. Nature *434*, 663–666.

Parker, J.S., Parizotto, E.A., Wang, M., Roe, S.M., and Barford, D. (2009). Enhancement of the seed-target recognition step in RNA silencing by a PIWI/MID domain protein. Mol. Cell *33*, 204–214.

Rajewsky, N., and Socci, N.D. (2004). Computational identification of microRNA targets. Dev. Biol. *267*, 529–535.

Reuter, J.S., and Mathews, D.H. (2010). RNAstructure: software for RNA secondary structure prediction and analysis. BMC Bioinformatics *11*, 129.

Rivas, F.V., Tolia, N.H., Song, J.J., Aragon, J.P., Liu, J., Hannon, G.J., and Joshua-Tor, L. (2005). Purified Argonaute2 and an siRNA form recombinant human RISC. Nat. Struct. Mol. Biol. *12*, 340–349.

Ross, P.D., and Sturtevant, J.M. (1960). The Kinetics of Double Helix Formation from Polyriboadenylic Acid and Polyribouridylic Acid. Proc. Natl. Acad. Sci. USA *46*, 1360–1365.

Ross, P.D., and Sturtevant, J.M. (1962). On the kinetics and mechanism of helix formation: The two stranded poly(A+U) complex from polyriboadenylic acid and polyribouridylic acid. J. Am. Chem. Soc. *84*, 4503–4507.

Sabin, L.R., Delás, M.J., and Hannon, G.J. (2013). Dogma derailed: the many influences of RNA on the genome. Mol. Cell *49*, 783–794.

Schirle, N.T., and MacRae, I.J. (2012). The crystal structure of human Argonaute2. Science *336*, 1037–1040.

Schirle, N.T., Sheu-Gruttadauria, J., and MacRae, I.J. (2014). Structural basis for microRNA targeting. Science *346*, 608–613.

Schwarz, D.S., Tomari, Y., and Zamore, P.D. (2004). The RNA-induced silencing complex is a $Mg^{2+}$-dependent endonuclease. Curr. Biol. *14*, 787–791.

Sheng, G., Zhao, H., Wang, J., Rao, Y., Tian, W., Swarts, D.C., van der Oost, J., Patel, D.J., and Wang, Y. (2014). Structure-based cleavage mechanism of Thermus thermophilus Argonaute DNA guide strand-mediated DNA target cleavage. Proc. Natl. Acad. Sci. USA *111*, 652–657.

Shin, C., Nam, J.W., Farh, K.K., Chiang, H.R., Shkumatava, A., and Bartel, D.P. (2010). Expanding the microRNA targeting code: functional sites with centered pairing. Mol. Cell *38*, 789–802.

Song, J.J., Liu, J., Tolia, N.H., Schneiderman, J., Smith, S.K., Martienssen, R.A., Hannon, G.J., and Joshua-Tor, L. (2003). The crystal structure of the Argonaute2 PAZ domain reveals an RNA binding motif in RNAi effector complexes. Nat. Struct. Biol. *10*, 1026–1032.

Song, J.J., Smith, S.K., Hannon, G.J., and Joshua-Tor, L. (2004). Crystal structure of Argonaute and its implications for RISC slicer activity. Science *305*, 1434–1437.

Swarts, D.C., Jore, M.M., Westra, E.R., Zhu, Y., Janssen, J.H., Snijders, A.P., Wang, Y., Patel, D.J., Berenguer, J., Brouns, S.J., and van der Oost, J. (2014).

DNA-guided DNA interference by a prokaryotic Argonaute. Nature *507*, 258–261.

Tang, G., Reinhart, B.J., Bartel, D.P., and Zamore, P.D. (2003). A biochemical framework for RNA silencing in plants. Genes Dev. *17*, 49–63.

Tomari, Y., and Zamore, P.D. (2005). Perspective: machines for RNAi. Genes Dev. *19*, 517–529.

Turner, D.H., and Mathews, D.H. (2010). NNDB: the nearest neighbor parameter database for predicting stability of nucleic acid secondary structure. Nucleic Acids Res. *38*, D280–D282.

Wang, Y., Juranek, S., Li, H., Sheng, G., Tuschl, T., and Patel, D.J. (2008a). Structure of an argonaute silencing complex with a seed-containing guide DNA and target RNA duplex. Nature *456*, 921–926.

Wang, Y., Sheng, G., Juranek, S., Tuschl, T., and Patel, D.J. (2008b). Structure of the guide-strand-containing argonaute silencing complex. Nature *456*, 209–213.

Wang, H.W., Noland, C., Siridechadilok, B., Taylor, D.W., Ma, E., Felderer, K., Doudna, J.A., and Nogales, E. (2009a). Structural insights into RNA processing by the human RISC-loading complex. Nat. Struct. Mol. Biol. *16*, 1148–1153.

Wang, Y., Juranek, S., Li, H., Sheng, G., Wardle, G.S., Tuschl, T., and Patel, D.J. (2009b). Nucleation, propagation and cleavage of target RNAs in Ago silencing complexes. Nature *461*, 754–761.

Wang, W., Yoshikawa, M., Han, B.W., Izumi, N., Tomari, Y., Weng, Z., and Zamore, P.D. (2014). The initial uridine of primary piRNAs does not create the tenth adenine that Is the hallmark of secondary piRNAs. Mol. Cell *56*, 708–716.

Wee, L.M., Flores-Jasso, C.F., Salomon, W.E., and Zamore, P.D. (2012). Argonaute divides its RNA guide into domains with distinct functions and RNA-binding properties. Cell *151*, 1055–1067.

Wetmur, J.G., and Davidson, N. (1968). Kinetics of renaturation of DNA. J. Mol. Biol. *31*, 349–370.

Xia, T., SantaLucia, J., Jr., Burkard, M.E., Kierzek, R., Schroeder, S.J., Jiao, X., Cox, C., and Turner, D.H. (1998). Thermodynamic parameters for an expanded nearest-neighbor model for formation of RNA duplexes with Watson-Crick base pairs. Biochemistry *37*, 14719–14735.

Zhang, Z., Revyakin, A., Grimm, J.B., Lavis, L.D., and Tjian, R. (2014). Single-molecule tracking of the transcription cycle by sub-second RNA detection. eLife *3*, e01775.